PAPER

Check for updates

Topical delivery of chemotherapeutic drugs using nano-hybrid hydrogels to inhibit post-surgical tumour recurrence†

Chendan Liu,‡[a] Yudi Ma,‡[a] Song Guo,[b] Bingfang He[a] and Tianyue Jiang [iD] *[a]

Residual microtumours after surgical resection leading to tumour relapse is one of the major challenges for cancer therapy. Herein, we developed a nano-hybrid oligopeptide hydrogel for topical delivery of a chemotherapeutic drug, docetaxel (DTX), to inhibit the post-surgical tumour recurrence. This nano-hybrid hydrogel (DTX-CTs/Gel) was prepared by encapsulating DTX in cell-penetrating peptide-modified transfersomes followed by embedment in an oligopeptide hydrogel. The obtained DTX-CTs/Gel showed paintable and injectable properties, and could support prolonged retention at the administrated sites after topical administration. DTX-CTs released from the hydrogel presented high skin and tumour penetration capabilities, and increased the accumulation of DTX in the cancer cells leading to enhanced cell death. We showed that the topical delivery of DTX using DTX-CTs/Gel efficiently slowed down the tumour relapse in post-surgical mouse melanoma and breast tumour models.

1. Introduction

Hydrogels are formed by a network of molecular chains with a large water-containing cavity.[1–3] Due to a host of unique characteristics including a highly porous architecture, tuneable flexibility and structural similarity to natural extracellular matrices, hydrogels have been used as a reservoir for drug delivery[4–7] and a scaffold for tissue engineering.[8–11] Spurred by the advances in nanotechnology, nano-hybrid hydrogels are increasingly developed by integrating the individual superiority of nanocarriers and hydrogels.[12–14] Nanocarriers can be physically embedded in the hydrogel matrix[15,16] or chemically crosslinked to the architectural network.[17–19] The association of nanocarriers, such as liposomes,[20–22] polymeric nanoparticles,[23,24] nanogels[25,26] and inorganic nanoparticles,[27–29] provides hydrogels with favourable properties and versatile functions. For example, a chitosan/dextran hybrid hydrogel loaded with silver nanoparticles showed higher antibacterial activity than the bare hydrogel, which significantly promoted the healing of the diabetic wound after topical administration.[30] Moreover, nano-hybrid hydrogels achieve a broader loading range and higher encapsulation

efficiency of drugs, particularly hydrophobic drugs that can be solubilized by nanocarriers.[31,32] In addition, the hybridization of nanoparticles can also improve the stiffness, elasticity and adhesiveness of the hydrogels.[33]

Herein, we developed a nano-hybrid oligopeptide hydrogel embedded with transfersomes for topical delivery of anticancer drugs to suppress the post-surgical tumour relapse (Fig. 1). Docetaxel (DTX), a hydrophobic small-molecule chemotherapeutic drug, is selected as a model drug. Transfersomes composed of phospholipid and surfactant are employed for the encapsulation of DTX. The surfactants as edge activators have the potential effect on elevating the transdermal efficiency by increasing the lipid fluidity of the stratum corneum and the deformability of the transfersomes.[34–36] The DTX-loaded transfersomes (DTX-Ts) are further modified with a cell-penetration peptide (CPP) consisting of octaarginine and trihistidine (R8H3) that has been found to be able to promote the skin and tumour penetration of transfersomes.[37–39] To enhance the tissue retention of the DTX-loaded CPP-modified transfersomes (DTX-CTs), we encapsulate DTX-CTs in an oligopeptide hydrogel as a depot. The oligopeptide hydrogel is formed by protease-catalytic self-assembly of short peptide-based building blocks, Fmoc-Phe (Fmoc-F) and Phe-Phe-Dopa (FF-Dopa) (Fig. 1a).[40,41] The obtained DTX-CTs-embedded hybrid oligopeptide hydrogel (DTX-CTs/Gel) has favourable paintability and injectability, and provides prolonged retention of DTX-CTs on/in the administered site. In this study, we evaluate the therapeutic efficacy of DTX-CTs/Gel as a topical delivery system of DTX in inhibiting post-surgical tumour

[a]*School of Pharmaceutical Sciences, Nanjing Tech University, Nanjing 211816, China. E-mail: tjiang@njtech.edu.cn*
[b]*Affiliated Hospital of Nanjing University of Chinese Medicine, Jiangsu Province Hospital of Chinese Medicine, Nanjing 210029, China*

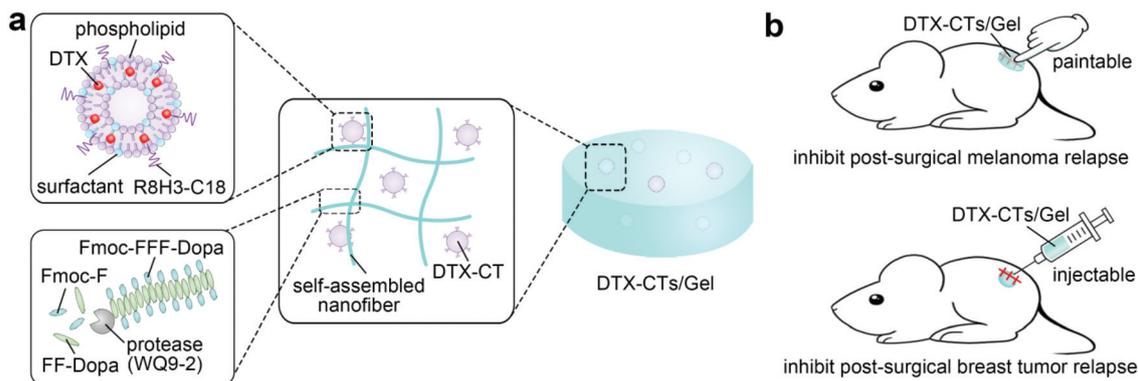‡These authors contributed equally to this work.

Fig. 1 (a) Schematic illustration of the structure of DTX-CTs/Gel. (b) Schematic illustration of the topical delivery of DTX using DTX-CTs/Gel for inhibiting the post-surgical melanoma and breast tumour relapse.

recurrence in mouse melanoma and breast tumour models (Fig. 1b).

2.   Experimental section

2.1.   Materials

DTX was obtained from Yew Pharmaceutical Co., Ltd. Soybean phospholipid was purchased from Tywei Pharm. Co., Ltd. Tween 80 was purchased from Sangon Biotech Co., Ltd. Span 80 and sodium deoxycholate were obtained from Sinopharm Chemical Reagent Co., Ltd. Stearyl R8H3 (R8H3-C18), Fmoc-F and FF-Dopa peptides were purchased from GL Biochem Co., Ltd. Coumarin 6 (Cou6) was purchased from Shanghai Aladdin Bio-Chem Technology Co., Ltd. WQ9-2 was expressed by our lab as previously described.[42,43]

2.2.   Preparation and characterization of transfersomes

The phospholipid and surfactants were dissolved in chloroform, followed by addition of DTX (5%, w:w). A lipid film formed by evaporating the organic solvent was hydrated with deionized water and subjected to ultrasonication in an ice bath. DTX-loaded transfersomes (DTX-Ts) were obtained after extrusion through a filter membrane with 220 nm pore size. DTX-CTs were obtained by incubating DTX-Ts with R8H3-C18 (2.5 mol%) at 4 °C for 30 min. To prepare fluorescent Cou6-loaded transfersomes (Cou6-Ts), Cou6 (0.2%, w:w) was added to the components. DTX was quantified using high-performance liquid chromatography (HPLC). The hydrodynamic diameter and zeta potential were analysed using a zetasizer (Malvern, Nano ZS90). Analysis of the DTX-CTs structure was performed on a transmission electron microscope (TEM) (Hitachi, HT7800). The entrapment efficiency and drug-loading capacity of DTX in DTX-CTs were calculated.

2.3.   Transdermal efficiency

The Franz diffusion experiment was carried out to evaluate the transdermal efficiency of the transfersomes. In brief, the mouse abdominal skin was harvested and deposited between donor and acceptor chambers. In the donor chamber, DTX-Ts were added on the surface of the skin, while in the acceptor chamber, PBS/ethanol medium (3 : 1, v:v) was filled. The acceptor chamber was incubated at 37 °C under stirring. At different time points, the medium was withdrawn and fresh medium (equal volume) was supplemented. DTX in the medium was quantified using HPLC. The cumulative amount of DTX permeating through the skin was calculated as follows:

$$Q_n = \left(VC_n + \sum_{i=1}^{n-1} C_i V_i \right)/S$$

where Q_n is the cumulative amount of DTX penetrating across the skin per cm^2; V and V_i are the capacities of the acceptor chamber (8 mL) and sampling volume (0.8 mL), respectively; C_n and C_i are the concentrations of DTX in the buffer in the acceptor chamber at different time points and at the ith ($n-1$) time point, respectively; S is the diffusion area of the skin. At 24 h, the skin was harvested, washed with hydroalcoholic solution (50%, v:v) and homogenized. After centrifugation, DTX in the supernatant was quantified using HPLC.

2.4.   *In vitro* cytotoxic effect

Mouse melanoma (B16F10) cells and human normal liver (L-02) cells were purchased from the Cell Bank of Chinese Academy of Sciences, while luciferase-tagged mouse triple negative breast cancer (4T1-Luc) cells were obtained from Prof. Chao Wang at Soochow University. B16F10 and 4T1-Luc cells were incubated with DTX-Ts and DTX-CTs at different DTX concentrations at 37 °C for 24 h, respectively. L-02 cells were incubated with the blank CTs at different concentrations at 37 °C for 24 h. The cells were then incubated with methyl thiazolyl tetrazolium solution (0.5 mg mL^{-1}) at 37 °C for another 4 h. Subsequently, dimethyl sulfoxide was added after removal of the solution. The absorbance of dimethyl sulfoxide solution was determined at a wavelength of 570 nm using a microplate reader (BioTek, PowerWave XS). The viability of the cells after different treatments was calculated.

2.5. Preparation and characterization of DTX-CTs/Gel

DTX-CTs (0.25 mL, 1 mg mL^{-1} DTX) were mixed with PBS (0.55 mL, pH 7.4) containing Fmoc-F (18.2 mM) and FF-Dopa precursors (36.4 mM). The WQ9-2 solution (0.2 mL) was then added to trigger the gel formation. The mixture was stabilized at 37 °C for 4 h to obtain DTX-CTs/Gel. The morphology of DTX-CTs/Gel was observed using a scanning electron microscope (SEM) (FEI, Quanta FEG250). For the rheology study, the modulus of the PBS solution containing transfersomes and precursors after the addition of WQ9-2 was measured (strain: 2%, frequency: 2 Hz) over time using a rheometer (Anton Paar, MCR302).

2.6. Animal and tumour models

C57BL/6 (male, 18–22 g) and Balb/C mice (female, 18–22 g) were provided by the Comparative Medicine Centre of Yangzhou University. All animal procedures were performed in accordance with the Guidelines for Care and Use of Laboratory Animals of Nanjing Tech University and approved by the Animal Ethics Committee of Nanjing Tech University. To establish mouse melanoma models, B16F10 cells were subcutaneously injected to the dorsum of C57BL/6 mice (1 × 10^6 cells per mouse). The tumour volume (length × width × width/2) was measured using a vernier calliper. To establish mouse melanoma resection models, the tumour was surgically removed at day 6 after the implantation of B16F10 cells, and the tumour volume was measured. To establish mouse breast tumour resection models, 4T1-Luc cells were subcutaneously injected into the mammary fat pad of Balb/C mice (1 × 10^6 cells per mouse), and the tumour was surgically removed at day 10 after the implantation of 4T1-Luc cells. The luminescent signals from 4T1-Luc were monitored, indicating the tumour growth and post-surgical recurrence. The mice received an intraperitoneal injection of D-luciferin (150 mg kg^{-1}), and were then analysed using an *in vivo* imaging system (IVIS) (PerkinElmer, Spectrum) at 0.25 h after injection.

2.7. *In vivo* skin and tumour penetration

B16F10 tumour-bearing mice were topically painted with Cou6-Ts/Gel and Cou6-CTs/Gel onto the skin above the tumour once a day, respectively. After 3 days of treatment, the skin with the tumour was removed and treated by freezing microtomy. The frozen tissue section was stained with DAPI, and then observed using a fluorescence microscope (Nikon Eclipse Ci).

2.8. *In vivo* therapeutic efficacy in mouse melanoma models

B16F10 tumour-bearing mice were topically painted with saline, DTX-CTs, DTX-Ts/Gel and DTX-CTs/Gel once a day (8 times), respectively. The administration dosage of DTX was 1 mg kg^{-1}. The tumour volume and body weight were measured during the treatment. After the treatment, the tumours were removed and treated by freezing microtomy. The frozen tumour section was stained using the TUNEL apoptosis assay kit (Roche), and then observed using a fluorescence

microscope (Nikon Eclipse Ci). To evaluate the anti-relapse effect, ~99% of tumours were surgically removed with ~1% remaining to mimic the residual microtumours after surgery.[44] Sterile instruments were used on the anaesthetized mice during the surgical process. The surgically-treated tumour-bearing mice were topically painted with saline, DTX-CTs, DTX-Ts/Gel and DTX-CTs/Gel on the wound skin once a day (8 times), respectively. The tumour volume and body weight were measured during the treatment.

2.9. *In vivo* therapeutic efficacy in mouse breast tumour resection models

At day 10 after implantation of 4T1-Luc cells, ~99% of tumours were surgically removed with ~1% remaining to mimic the residual microtumours after surgery. Sterile instruments were used on the anaesthetized mice during the surgical process. The surgically-treated tumour-bearing mice received a single intratumoural injection of saline, DTX-CTs, DTX-Ts/Gel and DTX-CTs/Gel, respectively. The administration dosage of DTX was 1 mg kg^{-1}. The mice were imaged using IVIS (PerkinElmer). The tumour and body weight were measured, and the survival was recorded.

2.10. Statistical analysis

All the data are presented as mean ± standard deviation. One-way analysis of variance (ANOVA) was applied for statistical comparisons of multiple groups. *$P < 0.05$ indicates statistical significance.

3. Results and discussion

3.1. Preparation and characterization of DTX-CTs

The transfersomes composed of phospholipid and surfactants were prepared using the thin-film dispersion method. The surfactants as edge activators were introduced to the formulation for increased deformability of lipid layers and enhanced transdermal efficiency. Different DTX-Ts formulations containing three commonly-used edge activators, tween, span and sodium deoxycholate, were obtained and characterized (Tables S1 and S2†). The particle size of the obtained DTX-Ts ranged from 60 to 100 nm. The incorporation of sodium deoxycholate, an anionic surfactant, resulted in negatively charged DTX-Ts, while the introduction of a non-ionic surfactant, Tween 80 and Span 80, provided DTX-Ts with neutral surface charge.

The transfersomes have been demonstrated to show superior transdermal capacity compared to the liposomes. To evaluate the impact of the incorporated edge activators on the skin penetration of the transfersomes, the transdermal efficiency of the transfersomes was investigated using the Franz diffusion cell system (Fig. 2a). Compared with the liposomes (F0), all the transfersomes (F1–F5) showed an increased transdermal efficiency, which is attributed to the effects of edge activators on increasing the lipid fluidity of the stratum corneum and improving the deformability of transfersomes. Notably, DTX-Ts with Tween 80 (F3) showed higher transder-
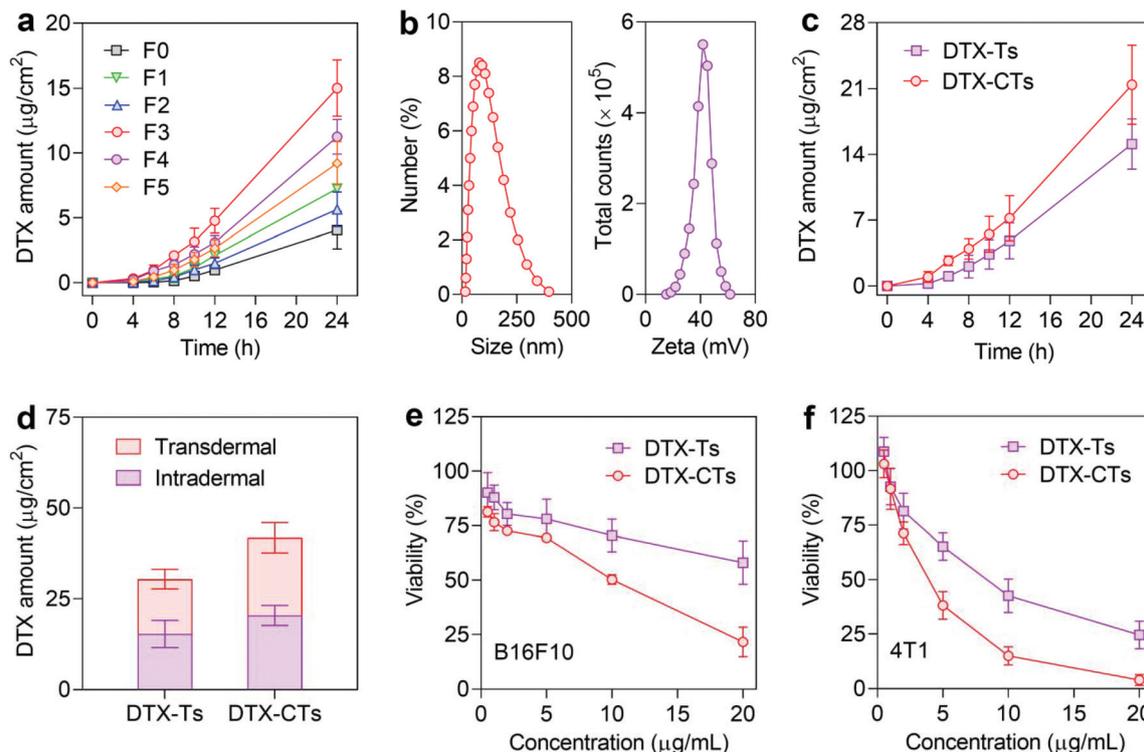
Fig. 2 (a) Transdermal amounts of DTX after the mouse skin was treated with different DTX formulations over time. F0 was the DTX-loaded liposomes without surfactants, while F1–F5 were the DTX-loaded transfersomes with different amounts of surfactants (F1: 10% sodium deoxycholate; F2: 10% Span 80; F3: 10% Tween 80; F4: 10% Tween 80 + 10% sodium deoxycholate; F5: 10% Tween 80 + 10% Span 80). (b) Particle size (left) and zeta potential (right) distribution curves of DTX-CTs. (c) Transdermal amounts of DTX after the mouse skin was treated with DTX-Ts and DTX-CTs over time. (d) Transdermal and intradermal amounts of DTX after the mouse skin was treated with DTX-Ts and DTX-CTs for 24 h. (e,f) Viabilities of B16F10 and 4T1-Luc cells after treatment with different concentrations of DTX-Ts and DTX-CTs for 24 h.

mal efficiency than that with either sodium deoxycholate (F1) or Span 80 (F2). The average cumulative amounts of DTX permeating through the skin within 24 h were 7.25 (F1), 5.65 (F2), and 15.0 (F3) $\mu g\ cm^{-2}$, respectively. Moreover, the combination of Tween 80 with sodium deoxycholate (F4) or Span 80 (F5) at the studied concentrations did not increase the transdermal efficiency. Collectively, DTX-Ts containing Tween 80 performed efficient transdermal delivery of DTX.

We further modified DTX-Ts with the R8H3 peptide for enhanced transdermal permeation. R8H3, a cell-penetrating peptide, has been demonstrated to increase both skin and tumour penetration of nanocarriers.[37–39] The obtained DTX-CTs had a comparable size of ~79 nm to DTX-Ts, but a positive surface charge of ~+42 mV due to the modification of the cationic R8H3 peptide (Fig. 2b). The TEM image of DTX-CTs displayed a spherical shape with a unique vesicular structure (Fig. S1†). The encapsulation efficiency and drug-loading capacity of DTX in DTX-CTs were about 89.4% and 4.7%, respectively. As expected, DTX-CTs markedly promoted the skin penetration of DTX compared with DTX-Ts. The average cumulative transdermal amounts of DTX delivered by DTX-CTs increased to 21.4 $\mu g\ cm^{-2}$ within 24 h (Fig. 2c). In addition, the intradermal amount of DTX in the DTX-CTs-treated group after 24 h of treatment was also higher than that

in the DTX-Ts-treated group (Fig. 2d), indicating that DTX-CTs exhibit more infiltration into the skin and therefore enhanced transdermal penetration of DTX.

To further validate whether the R8H3 peptide modification promoted the tumour cell penetration and increased the intratumoural concentration for enhanced anticancer activity of DTX, the *in vitro* cytotoxicities of DTX-CTs against B16F10 and 4T1-Luc cells were assessed, respectively. DTX-CTs showed a higher cytotoxic effect on both cancer cell models than DTX-Ts (Fig. 2e and f). The half-maximal inhibitory concentration (IC50) of DTX-CTs was 7.46 $\mu g\ mL^{-1}$ on B16F10 cells and 3.72 $\mu g\ mL^{-1}$ on 4T1-Luc cells, much lower than 21.80 $\mu g\ mL^{-1}$ and 8.38 $\mu g\ mL^{-1}$ of DTX-Ts. In addition, the bare CTs exhibited no significant cytotoxicity on L-02 cells at all the tested concentrations (Fig. S2†). These data indicate that DTX-CTs increase the intracellular concentration of DTX and cause enhanced cytotoxicity against cancer cells.

3.2. Preparation and characterization of DTX-CTs/Gel

To realize prolonged retention of DTX-CTs at the administration site after topical administration, the oligopeptide hydrogel was selected as a semisolid reservoir for the encapsulation and local delivery of DTX-CTs. The protease-catalytic self-assembly strategy was employed for the formation of the
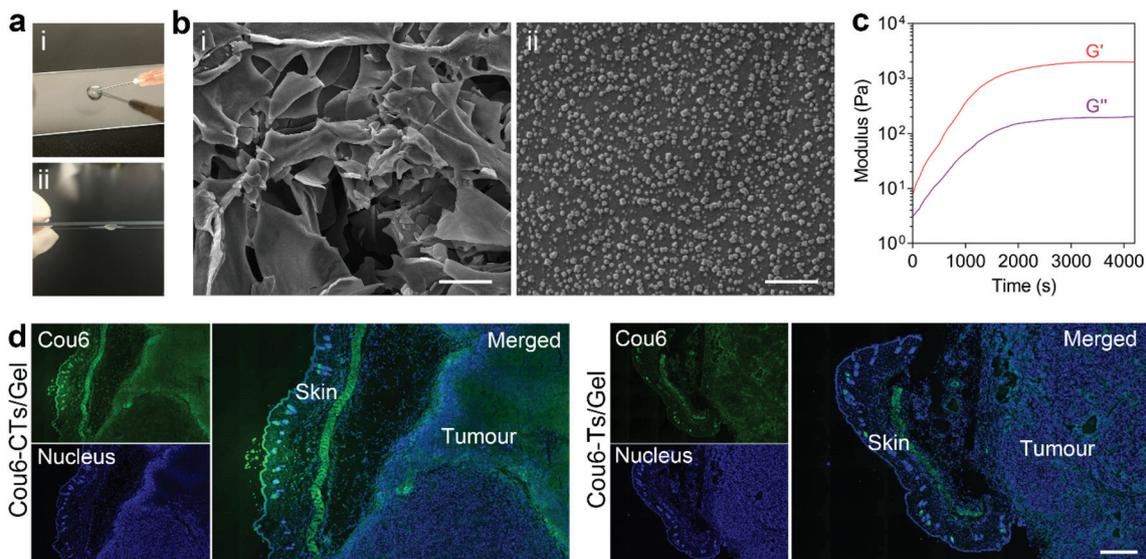
Fig. 3 (a) Injectability of DTX-CTs/Gel. (i) DTX-CTs/Gel could be injected through a syringe; (ii) DTX-CTs/Gel could recover shortly after injection. (b) SEM images of DTX-CTs/Gel. (i) Low magnification; (ii) high magnification. Scale bars are 50 μm (i) and 500 nm (ii). (c) Rheology of DTX-CTs/Gel after the addition of WQ9-2. *G′*: storage modulus; *G″*: loss modulus. (d) Fluorescence images of the skin with the tumour tissue section after treatment with Cou6-CTs/Gel and Cou6-Ts/Gel. Scale bar is 1 mm.

oligopeptide hydrogel. The addition of the WQ9-2 protease to the DTX-CTs solution containing Fmoc-F and FF-Dopa precursors led to the generation of the Fmoc-FFF-Dopa gelator, which could self-assemble into nanofibers *via* non-covalent interactions and form the nano-hybrid hydrogel, DTX-CTs/Gel.

The obtained DTX-CTs/Gel possessed injectability(Fig. 3a) since the non-covalent interactions between gelators drive the self-assembly and can recover shortly after injection. The SEM images showed that the microscale structure of DTX-CTs/Gel was supported by the crosslinked network, and DTX-CTs were
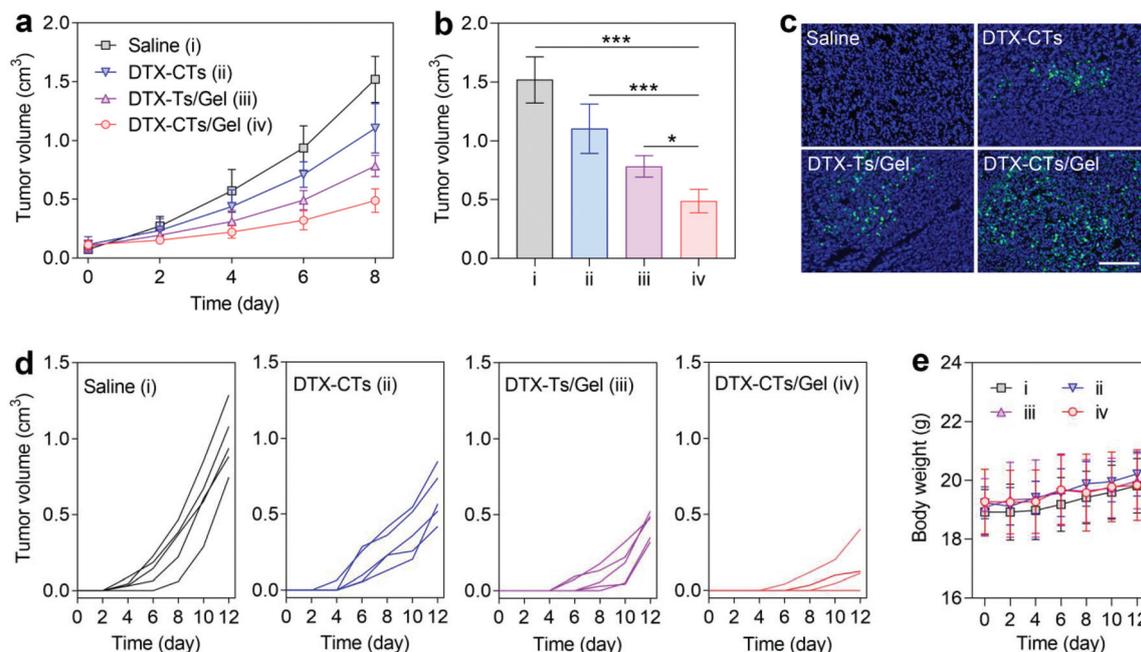

Fig. 4 (a) B16F10 tumour growth curves of the tumour-bearing mice after different treatments. (b) Tumour volumes at day 8 after different treatments. *P < 0.05 and ***P < 0.001. (c) Fluorescence images of the tumour tissues stained with TUNEL at day 8 after different treatments. Scale bar is 100 μm. (d) Individual B16F10 tumour growth curves of the surgically-treated tumour-bearing mice after different treatments. (e) Mouse body weight change curves after different treatments.

observed to be encapsulated in the hydrogel (Fig. 3b). The rheology of the precursor solution after adding WQ9-2 was investigated. The addition of WQ9-2 triggered a significant increase in the values of G' (storage modulus) and G'' (loss modulus) *versus* time (Fig. 3c). The G' value reached a plateau of about 2000 Pa, up to 10-fold of the G'' value, indicating the formation of a self-supporting hydrogel with strong mechanical force.

Next, we evaluated the *in vivo* transdermal efficiency of CTs delivered by the paintable oligopeptide hydrogel. Cou6, a fluo-

rescent dye, was encapsulated into CTs for fluorescence tracing. The B16F10 tumour-bearing mice were topically painted with Cou6-CTs/Gel on the skin melanoma, once a day for 3 days. Subsequently, the distribution of Cou6-CTs in the treated skin and tumour tissue was observed by means of freezing microtomy and confocal microscopy (Fig. 3d). The fluorescence images showed that treatment with Cou6-CTs/Gel resulted in a high Cou6 fluorescent signal distributing in both the skin layer and tumour site. By comparison, the Cou6 fluorescent signal was obviously weaker at both the skin layer and tumour site
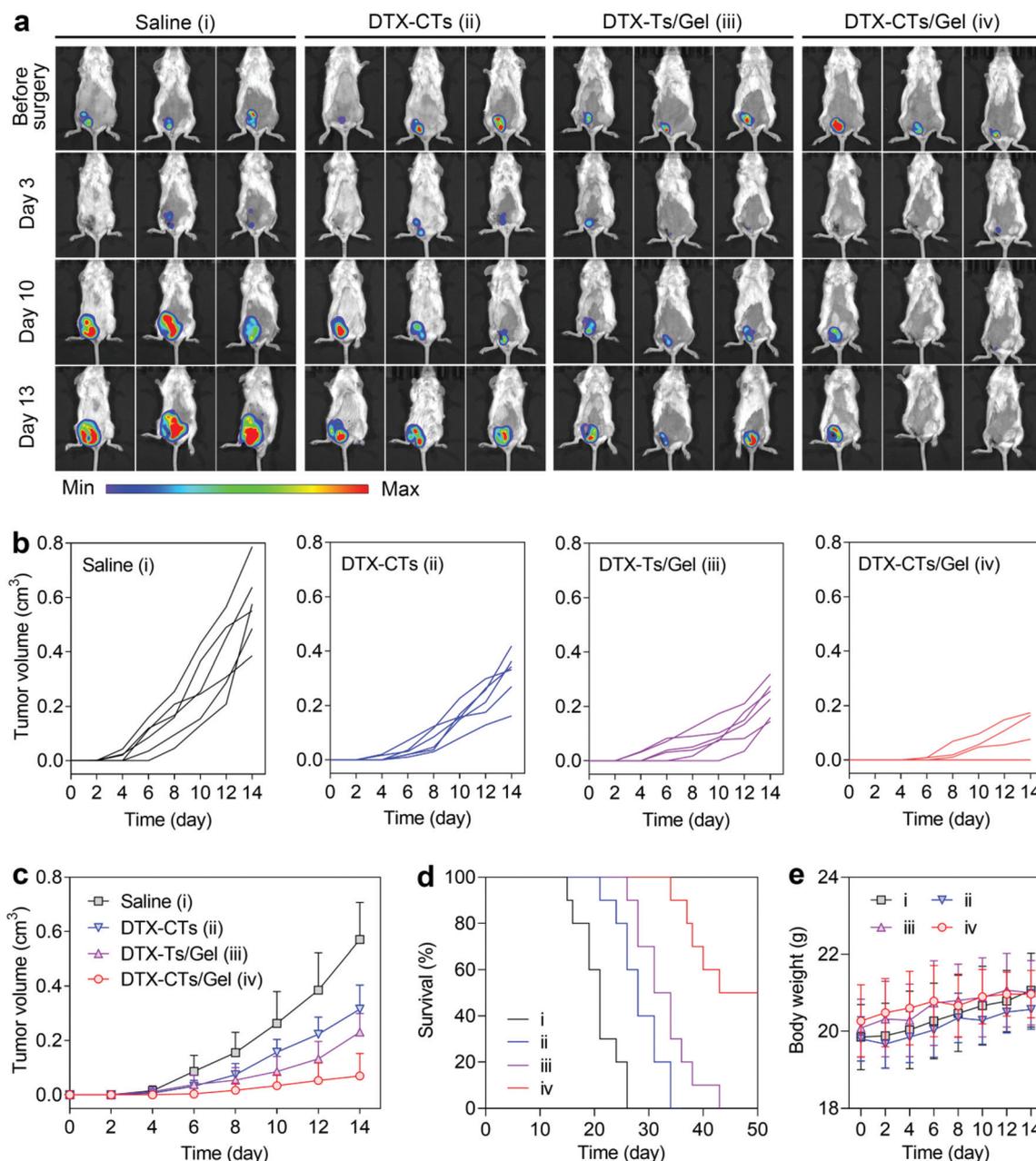

Fig. 5 (a) Luminescence images of the surgically-treated 4T1-Luc tumour-bearing mice after different treatments. (b and c) Individual (b) and average (c) 4T1-Luc tumour growth curves of the surgically-treated tumour-bearing mice after different treatments. (d and e) Survival (d) and body weight change (e) curves of the surgically-treated tumour-bearing mice after different treatments.

after the Cou6-Ts/Gel treatment, suggesting that CTs/Gel showed an enhanced skin and tumour penetration capability. The results indicate that the paintable oligopeptide hydrogel allows CTs to stick to the skin for a long time period, and the released CTs from the hydrogel promoted the chemotherapeutic drugs to cross the skin and penetrate the tumour.

3.3. *In vivo* therapeutic efficacy on the inhibition of tumour growth and recurrence

We first evaluated the *in vivo* anticancer activity of the paintable DTX-CTs/Gel in suppressing the growth of primary melanoma after topical administration on the skin. As shown in Fig. 4a, the primary B16F10 tumour growth was significantly inhibited by successive skin plastering of the DTX formulations including DTX-CTs, DTX-Ts/Gel and DTX-CTs/Gel. As expected, DTX-CTs/Gel produced a significantly higher tumour-inhibiting effect than the DTX-CTs solution, which results from the enhanced skin retention of DTX-CTs with long-term acting properties provided by the hydrogel. Moreover, DTX-CTs/Gel also showed a greater effect on inhibiting tumour growth than DTX-Ts/Gel, which is mainly due to the increased penetration of DTX from the skin to the tumour supported by CTs. Treatment with DTX-CTs/Gel resulted in the smallest tumour size (Fig. 4b) and the most apoptotic cells in the tumour tissue (Fig. 4c).

Next, we assessed the therapeutic efficacy of DTX-CTs/Gel in inhibiting the post-surgical melanoma recurrence after topical administration on the wound skin. After surgical removal of the primary B16F10 tumour (~99%), the wound was sutured and plastered with saline, DTX-CTs, DTX-Ts/Gel and DTX-CTs/Gel, respectively. As shown in Fig. 4d, the mice receiving the treatment of DTX-CTs/Gel exhibited markedly delayed tumour relapse and the smallest volume of the recurrent tumour. In addition, two of five experimental mice in the DTX-CTs/Gel-treated group showed a strong therapeutic response without any detectable recurrent tumours with the studied time period. The treatment did not cause any impact on the body weight of the mice (Fig. 4e). In contrast, the mice treated with either DTX-CTs or DTX-Ts/Gel had a modest delay of tumour re-growth, but post-surgical tumour recurrence was not prevented in the surgical bed.

We further estimated the anti-relapse effect of DTX-CTs/Gel on the breast 4T1-Luc tumour resection model after intratumoural injection. After surgical removal of the primary 4T1-Luc tumour (~99%), the wound was sutured and injected with saline, DTX-CTs, DTX-Ts/Gel and DTX-CTs/Gel, respectively, and the mice were detected using IVIS. As shown in Fig. 5a, post-surgical tumour relapse was observed as high detected luminescent signals from the 4T1-Luc tumour after the saline treatment. All the mice treated with a single injection of DTX formulations slowed down the tumour recurrence. Treatment with DTX-CTs/Gel produced the greatest effect on suppressing the tumour relapse after surgery, as evidenced by the lowest luminescent signals. Meanwhile, the tumour volume was measured. The smallest recurrent tumour was determined after the DTX-CTs/Gel treatment (Fig. 5b and c), and no recur-

rent tumour was found in three of six experimental mice during the studied period (Fig. 5b). Moreover, the survival of the treated mice was monitored. The surgically-treated mice receiving the DTX-CTs/Gel treatment exhibited the longest survival period compared with that treated with either DTX-CTs or DTX-Ts/Gel (Fig. 5d). The body weights of the mice were not affected by the treatment (Fig. 5e).

4. Conclusions

In conclusion, we have developed DTX-CTs/Gel as a topical delivery system of DTX to suppress the recurrence of the tumour after surgical resection. DTX-CTs possessed high skin and tumour penetration efficiency, and showed increased cytotoxicity against tumour cells. DTX-CTs/Gel showed favourable paintable and injectable properties, and could be conveniently applied for local administration. We showed that the topical delivery of DTX using DTX-CTs/Gel efficiently slowed down the tumour relapse in both post-surgical mouse melanoma and breast tumour models. These findings encourage the potential clinical translation of this nano-hybrid hydrogel-mediated topical delivery of chemotherapeutic drugs for post-surgical adjunctive therapy. Large animal studies are expected for formulation optimization, dosage adjustment, treatment schedule and therapeutic efficacy.

Conflicts of interest

There are no conflicts to declare.

Acknowledgements

References

1 W. E. Hennink and C. F. van Nostrum, *Adv. Drug Delivery Rev.*, 2002, **54**, 13–36.
2 J. Elisseeff, *Nat. Mater.*, 2008, **7**, 271–273.
3 E. M. Ahmed, *J. Adv. Res.*, 2015, **6**, 105–121.
4 M. Norouzi, B. Nazari and D. W. Miller, *Drug Discovery Today*, 2016, **21**, 1835–1849.
5 T. Thambi, Y. Li and D. S. Lee, *J. Controlled Release*, 2017, **267**, 57–66.
6 J. Tan, M. Zhang, Z. Hai, C. Wu, J. Lin, W. Kuang, H. Tang, Y. Huang, X. Chen and G. Liang, *ACS Nano*, 2019, **13**, 5616–5622.

7 J. E. Sun, B. Stewart, A. Litan, S. J. Lee, J. P. Schneider, S. A. Langhans and D. J. Pochan, *Biomater. Sci.*, 2016, **4**, 839–848.

8 Q. Huang, Y. Zou, M. C. Arno, S. Chen, T. Wang, J. Gao, A. P. Dove and J. Du, *Chem. Soc. Rev.*, 2017, **46**, 6255–6275.

9 J. Yang, Y. S. Zhang, K. Yue and A. Khademhosseini, *Acta Biomater.*, 2017, **57**, 1–25.

10 Q. Li, C. Liu, J. Wen, Y. Wu, Y. Shan and J. Liao, *Chin. Chem. Lett.*, 2017, **28**, 1857–1874.

11 Y. Li, X. Wang, Y. Wei and L. Tao, *Chin. Chem. Lett.*, 2017, **28**, 2053–2057.

12 P. Thoniyot, M. J. Tan, A. A. Karim, D. J. Young and X. J. Loh, *Adv. Sci.*, 2015, **2**, 1400010.

13 W. Gao, Y. Zhang, Q. Zhang and L. Zhang, *Ann. Biomed. Eng.*, 2016, **44**, 2049–2061.

14 W. Gao, D. Vecchio, J. Li, J. Zhu, Q. Zhang, V. Fu, S. Thamphiwatana, D. Lu and L. Zhang, *ACS Nano*, 2014, **8**, 2900–2907.

15 C. Dannert, B. T. Stokke and R. S. Dias, *Polymers*, 2019, **11**, 275.

16 F. ud Din, O. Mustapha, D. W. Kim, R. Rashid, J. H. Park, J. Y. Choi, S. K. Ku, C. S. Yong, J. O. Kim and H.-G. Choi, *Eur. J. Pharm. Biopharm.*, 2015, **94**, 64–72.

17 S. Yan, J. Ren, Y. Jian, W. Wang, W. Yun and J. Yin, *Biomacromolecules*, 2018, **19**, 4554–4564.

18 R. Yegappan, V. Selvaprithiviraj, A. Mohandas and R. Jayakumar, *Colloids Surf., B*, 2019, **177**, 41–49.

19 B. Tao, C. Lin, Y. Deng, Z. Yuan, X. Shen, M. Chen, Y. He, Z. Peng, Y. Hu and K. Cai, *J. Mater. Chem. B*, 2019, **7**, 2534–2548.

20 H. Y. Yoon, I. H. Chang, Y. T. Goo, C. H. Kim, T. H. Kang, S. Y. Kim, S. J. Lee, S. H. Song, Y. M. Whang and Y. W. Choi, *Int. J. Nanomed.*, 2019, **14**, 6249–6268.

21 M. T. Popescu, S. Mourtas, G. Pampalakis, S. G. Antimisiaris and C. Tsitsilianis, *Biomacromolecules*, 2011, **12**, 3023–3030.

22 Z. Chen, F. Liu, Y. Chen, J. Liu, X. Wang, A. T. Chen, G. Deng, H. Zhang, J. Liu and Z. Hong, *Adv. Funct. Mater.*, 2017, **27**, 1703036.

23 S. Merino, C. Martin, K. Kostarelos, M. Prato and E. Vazquez, *ACS Nano*, 2015, **9**, 4686–4697.

24 S. Shen, X. Xu, S. Lin, Y. Zhang, H. Liu, C. Zhang and R. Mo, *Nat. Nanotechnol.*, 2021, **16**, 104–113.

25 T. Zhang, R. Yang, S. Yang, J. Guan, D. Zhang, Y. Ma and H. Liu, *Drug Delivery*, 2018, **25**, 278–292.

26 J. Zhu, F. Li, X. Wang, J. Yu and D. Wu, *ACS Appl. Mater. Interfaces*, 2018, **10**, 13304–13316.

27 J. Stojkovska, J. Zvicer and B. Obradovic, *Appl. Microbiol. Biotechnol.*, 2020, **104**, 4643–4658.

28 D. Lee, D. N. Heo, H. R. Nah, S. J. Lee, W. K. Ko, J. S. Lee, H. J. Moon, J. B. Bang, Y. S. Hwang, R. L. Reis and I. K. Kwon, *Int. J. Nanomed.*, 2018, **13**, 7019–7031.

29 N. Masood, R. Ahmed, M. Tariq, Z. Ahmed, M. S. Masoud, I. Ali, R. Asghar, A. Andleeb and A. Hasan, *Int. J. Pharm.*, 2019, **559**, 23–36.

30 G. Shi, W. Chen, Y. Zhang, X. Dai, X. Zhang and Z. Wu, *Langmuir*, 2019, **35**, 1837–1845.

31 T. Tanigo, R. Takaoka and Y. Tabata, *J. Controlled Release*, 2010, **143**, 201–206.

32 M. Narvekar, H. Y. Xue, J. Y. Eoh and H. L. Wong, *AAPS PharmSciTech*, 2014, **15**, 822–833.

33 E. Piantanida, G. Alonci, A. Bertucci and L. De Cola, *Acc. Chem. Res.*, 2019, **52**, 2101–2112.

34 H. Marwah, T. Garg, A. K. Goyal and G. Rath, *Drug Delivery*, 2016, **23**, 564–578.

35 M. Ashtikar, K. Nagarsekar and A. Fahr, *J. Controlled Release*, 2016, **242**, 126–140.

36 M. Kong, L. Hou, J. Wang, C. Feng, Y. Liu, X. Cheng and X. Chen, *Chem. Commun.*, 2015, **51**, 1453–1456.

37 T. Jiang, T. Wang, T. Li, Y. Ma, S. Shen, B. He and R. Mo, *ACS Nano*, 2018, **12**, 9693–9701.

38 T. Jiang, Z. Zhang, Y. Zhang, H. Lv, J. Zhou, C. Li, L. Hou and Q. Zhang, *Biomaterials*, 2012, **33**, 9246–9258.

39 T. Jiang, R. Mo, A. Bellotti, J. Zhou and Z. Gu, *Adv. Funct. Mater.*, 2014, **24**, 2295–2304.

40 J. X. Xu, Z. Zhou, B. Wu and B. F. He, *Nanoscale*, 2014, **6**, 1277–1280.

41 T. Jiang, S. Shen, T. Wang, M. Li, B. He and R. Mo, *Nano Lett.*, 2017, **17**, 7447–7454.

42 J. Xu, M. Jiang, H. Sun and B. He, *Bioresour. Technol.*, 2010, **101**, 7991–7994.

43 J. Xu, Y. Zhuang, B. Wu, L. Su and B. He, *J. Biol. Inorg. Chem.*, 2013, **18**, 211–221.

44 Q. Chen, C. Wang, X. Zhang, G. Chen, Q. Hu, H. Li, J. Wang, D. Wen, Y. Zhang and Y. Lu, *Nat. Nanotechnol.*, 2019, **14**, 89–97.